3-2022

Bimodal Particle Distributions with Increased Thermal Conductivity for Solid Particles as Heat Transfer Media and Storage Materials

Chase E. Christen
Boise State University

Jesús Gómez-Hernández
Universidad Carlos III de Madrid

Todd P. Otanicar
Boise State University

Publication Information

Christen, Chase E.; Gómez-Hernández, Jesús; and Otanicar, Todd P. (2022). "Bimodal Particle Distributions with Increased Thermal Conductivity for Solid Particles as Heat Transfer Media and Storage Materials". *International Journal of Heat and Mass Transfer, 184*, 122250. https://doi.org/10.1016/j.ijheatmasstransfer.2021.122250

Bimodal Particle Distributions with Increased Thermal Conductivity for Solid Particles as Heat Transfer Media and Storage Materials

Chase E. Christen[a], Jesús Gómez-Hernández[b], and Todd P. Otanicar[a,*]

[a] Department of Mechanical and Biomedical Engineering, Boise State University, 1910 W University Dr, Boise, ID 83725, USA, E-mail: toddotanicar@boisestate.edu
[b] Department of Thermal and Fluid Engineering, Universidad Carlos III de Madrid, Av. Universidad 30, 28911, Leganés, Madrid, Spain

Abstract

Solid particles are being considered in several high temperature thermal energy storage systems and as heat transfer media in a variety of advanced power generation systems, particularly in concentrated solar power plants. The downside of such an approach is the low overall heat transfer coefficients caused by the inherently low thermal conductivity values of the low-cost solid media when coupled to heat exchanger for the power cycle working fluid. Choosing the right particle size distribution, emittance, and material of the solid media can all make a substantial difference in packed bed thermal conductivity. Current research though exclusively focuses on continuous unimodal distributions of particles. Here, we propose the use of a binary particle system with a bimodal size distribution to significantly increase packed bed thermal conductivity by reducing packed bed porosity. This is the first study related to ceramic solid particle heat transfer that has considered the thermal conductivity of non-unimodal size distributions at room and elevated temperatures. The following study found that for the binary particle system using Carbo particles CP 16/30 – CP 70/140 where the large particle volume fraction was 50% there was an 17-47% increase in packed bed thermal conductivity when compared with a nearly unimodal particle size distribution of CP 16/30 between 50-300 ℃. Two different porosity and effective thermal conductivity models were studied, with one providing better prediction of porosity but both effective thermal conductivity models providing less predictive capacity. Importantly this approach can have a substantial impact of thermal performance, with little to no impact on the particle cost.

Keywords: Particle, Thermal Conductivity, Thermal Energy Storage, Moving Packed Bed

1. Introduction

Particles as a means for energy storage and heat transfer media have recently garnered more interest in fields such as energy conversion. High-temperature particle thermal energy storage has become a topic of interest due to the potential ability to have flexible power generation for durations of 10 to 100 hours [1]. Solid particles are a promising heat transfer media due to its ability to exceed temperatures of 1000 ℃. With the right heat exchanger design, solid particles could help run advanced power cycles that use high pressure (≥ 20 MPa) and high temperature (≥ 700 ℃) supercritical carbon dioxide (sCO_2) Brayton cycles to generate electricity [2,3]. As a result, there has been many research studies around developing low-cost thermal energy storage for particles as the heat transfer media particularly for the concentrating solar power (CSP) industry [2,4–6]. While solid particles hold promise for meeting low cost targets for energy storage and heat transfer fluids [3,4,7], current flowing packed bed heat exchangers suffer from low overall heat transfer coefficients as a result of low packed bed thermal conductivity [8,9]. While many studies considering moving packed bed systems, static packed bed thermal conductivity is relevant for a number of applications where the particle system isn't flowing such as in storage for industrial process heat [10], transparent packed bed solar receivers [11], and improving the packed bed thermal conductivity in static packed beds would also be of benefit [12]. This study proposes that binary particle systems, a mixture of two continuous unimodal particle systems leading to a continuous bimodal size distribution, can be used to significantly increase packed bed thermal conductivity at elevated temperatures; and thus, increase the heat transfer efficiency of moving packed bed heat exchangers.

While this paper will make the case for using binary particle systems, recent high-temperature experiments [8,9] and recently developed moving packed bed heat exchanger models [13,14] have only considered monodisperse particle systems, which is defined in this paper as a continuous unimodal distribution of particles, with diameters between 100-1000 μm. To understand why a binary particle system could increase heat exchanger performance, the terms of the overall heat transfer coefficient of the shell-and-plate moving packed bed heat exchanger must be understood. Albrecht and Ho define the overall heat transfer coefficient for a shell-and-plate moving packed bed heat exchanger as follows [13]:

$$U = \left(\frac{1}{\bar{h}_{CO_2}} + \frac{t_m}{k_m} + R_c^{"} + \frac{1}{\bar{h}_{sw}} \right)^{-1} \quad (1)$$

where $\bar{h}_{CO_2}$ is the average sCO_2 convection coefficient, t_m is the heat exchanger wall thickness, k_m is the heat exchanger material thermal conductivity, $R_c^{"}$ is the particle-wall contact resistance, and $\bar{h}_{sw}$ is the average particle-wall convection coefficient. Both near-wall contact resistance and the particle-wall convection coefficient are functions of the packed bed thermal conductivity[15]:

$$R_c^{"} = \frac{d_p}{2k_{s,eff}^{nw}} \tag{2}$$

$$\overline{Nu}_{Dh,H} = \frac{2w_{ch}\bar{h}_{sw}}{k_{s,eff}} = \left[\left(2\frac{0.886}{\sqrt{Gz^{-1}}}\right)^{\frac{12}{5}} + 12^{\frac{12}{5}}\right]^{\frac{5}{12}} \tag{3}$$

where d_p is the particle diameter, $k_{s,eff}^{nw}$ is the near-wall particle thermal conductivity, w_{ch} is the width of the particle channel, $k_{s,eff}$ is the effective bulk thermal conductivity of the packed bed, and Gz^{-1} is the inverse Graetz number ($Gz^{-1} = L/Pe_{Dh}D_h$). The inverse Graetz number is a function of the heat exchanger length (L), the Peclet number ($Pe_{D_h} = v_s D_h/\alpha$), and the hydaulic diameter of the particle flow ($D_h = 2w_{ch}$). An increase in the packed bed thermal conductivity could decrease the particle-wall contact resistance while also increasing the average particle-wall convection coefficient. The authors‘ goal in this study is to determine if binary particle systems lead to a substantial increase in packed bed thermal conductivity, a result that would warrant future packed bed and moving packed bed heat exchanger studies considering additional bimodal or binary particle distributions. Information about each term in the overall heat transfer coefficient, which won’t be described in this study, can be found in the following sources [13,15–21].

Bauman and Zunft previously studied the thermal properties of many different granular materials options for CSP systems [22]; however, their study only included two particles with the volumetric mean diameters under 1000 μm: 560 μm sintered bauxite & 800 μm quartz sand. This study expands on Bauman and Zunft’s research not only by measuring the thermal conductivity of five CARBO brand ceramic particles between 100-1000 μm, but this study also explores the benefit of using a bimodal particle distribution to increase packed bed thermal conductivity.

The idea of exploring binary particle systems can be seen by studying the Zehner, Bauer, and Schlünder (ZBS) (for example) thermal conductivity model [23]. The ZBS model is built

on a unit cell designed for spherical packings. The effective thermal conductivity of the packed bed is described as follows:

$$\frac{k_{s,eff}}{k_f} = \left(1-\sqrt{1-\varepsilon}\right)\varepsilon\left[\left(\varepsilon - 1 + \frac{1}{\kappa_G}\right)^{-1} + \kappa_r\right] + \sqrt{1-\varepsilon}[\varphi\kappa + (1-\varphi)k_c] \quad (4)$$

where k_f is the gas thermal conductivity, ε is the packed bed porosity, κ_G is the gas conduction ratio in the Knudsen regime, κ_r is the radiation ratio parameter, κ is a dimensionless parameter, k_c is a conduction term, and φ is an empirical contact parameter. The first term of the ZBS model includes the portion of the unit cell that only contains the fluid phase where the heat transfer consists of molecular conduction and radiation. The second equation consists of both solid and fluid phase, where one portion of heat transfer is due to surface contact while the second portion consists of conductive, convective, and radiative heat transfer. The preceding paragraph will describe the parameters that change the packed bed thermal conductivity according to the ZBS model. Researchers interested in learning more about the ZBS model are directed to Van Antwerpen's comprehensive review [24]. A recent review of effective thermal conductivities in packed beds also provides information on impacts to system performance[25].

Particle emissivity, particle size, solid particle conductivity, and packed bed porosity are the four parameters that can be modified to change packed bed thermal conductivity. Larger particle emissivity causes an increase in packed bed thermal conductivity; however, there is limited room for improvement by focusing on emissivity because CARBO ceramic particles already have an emissivity of 0.9 [26]. Baumann and Zunft demonstrated that larger particles improve packed bed thermal conductivity at higher temperatures primarily due to an increase in radiation [22]; however, larger particle diameters require wider particle channels to meet flowability requirements [13]. There will need to be more modeling and experiments before an optimal particle size distribution can be determined for moving packed bed heat exchangers. Bauman and Zunft found that choosing a particle with higher solid thermal conductivity can only marginally improve packed bed thermal conductivity [22]; therefore, using a high-cost material such as aluminum would not be justified compared to a low-cost material such as sand. Additionally, the cost of solid metal particles would be substantially higher making them impractical for many energy production purposes. Finally, thermal conductivity can be increased by decreasing packed bed porosity [27]. While monodisperse particles have a relatively constant porosity for diameters larger than 100 μm [28], a significant decrease in packed bed porosity can be achieved by using a binary packed bed [29]. Table 1 demonstrates

how porosity can make a substantial difference in packed bed thermal conductivity. Compared to all other properties, porosity caused the greatest increase in packed bed thermal conductivity when decreased to 0.36. For this reason, the authors believe that exploring binary particle systems is the most promising way of increasing packed bed thermal conductivity at little to no cost.

While previous articles focus on monodisperse particle systems with particle sizes from 350-3000 μm, this is the first study to broadly characterize the use of bimodal particle distributions at elevated temperatures for thermal energy storage and for solid particles as heat transfer media. This study investigates three different binary particle systems with varying size ratios that were fabricated across a wide range of large particle volume fractions with particles diameters between 100-1000 μm. The upcoming sections will cover the experimental methods including material selection and the measurement techniques for both porosity and thermal conductivity. Following that will be a description of the two different porosity models and two widely utilized thermal conductivity models used in this paper. Finally, the results will be presented and discussed, and future work is suggested.

2. Experimental Methods

2.1 Material Selection

Five CARBO ceramic particles were selected for investigation in this study: CP 16/30, CP 40/100, CP 70/140, HSP 16/30, and HSP 40/70. While sand has also been considered as a potential granular material in moving packed bed heat exchangers, the following study only considers CARBO ceramic particles due to their use in multiple previous models and experiments [8,13,14,30]. CARBO ceramic particles are popular due to the availability of many sizes, relative low cost, high durability, high sphericity, and good absorptive properties.

Binary particle systems of CP 16/30 – CP 40/100, CP 16/30 – CP 70/140, and HSP 16/30 – HSP 40/70 were assembled with large particle volume fractions (X_L) of 0.0, 0.25, 0.50, 0.75, or 1.0. Note that when X_L is either 0.0 or 1.0, the distribution is the monodisperse particle system for the fine and coarse particle in the mixture, respectively. In total, nine binary particle systems and five monodisperse particle systems were created. The particle size distributions for the monodisperse particle systems were either provided by CARBO with the particles or found on the company‘s data sheet [31]. While previous research has shown that there was no significant difference in size when compared to the optical microscopy measurements for three

CARBOBEAD CP particle systems [32] simultaneous measurements using an optical image and ImageJ processing software were made and are presented in Table 2. The optical analysis conducted here also resulted in a similar finding, with some differences for the CP 40/100 and CP 70/140 particles. The bimodal size distributions of the binary particle systems were calculated as follows:

$$Q_{i,binary} = X_L Q_{i,L} + (1 - X_L) Q_{i,s} \tag{5}$$

where $Q_{i,L}$ is the volume fraction of the coarse component, $Q_{i,s}$ is the volume fraction of the fine component, and X_L is the large particle volume fraction. The particle size distribution, particle size ratio, particle density, Sauter mean diameter, and average measured diameter for each particle sample in this study is shown in Table 2. It should be noted that only the single particle systems were characterized with the optical measurement. Further, since the mixtures were made based on the established sizes and mass measurements the distributions represented in Figure 1 are used for further calculations. Table A.1 in the appendix provides more details of the size distributions used in this study. The Sauter mean diameter, which is used for both porosity and thermal conductivity models, was calculated using the particle size distributions as described by Tsotsas and Schlünder for particles with the same shape and thermal conductivity [27]:

$$d_p = \left(\sum_{i=1}^{n} \frac{Q_i}{d_i} \right)^{-1} \tag{6}$$

where Q_i is the volume fraction of the particle for a given sieve size, and d_i is the mean particle diameter of a given bin.

2.2 Porosity Measurement Methods

Because decreasing packed bed porosity was found to be the main driver in increasing the thermal conductivity of a multigranular packed beds [27], three binary particle systems were chosen so that a large change in porosity would be observed. It has been shown that lower size ratios (r), the ratio of the Sauter mean diameter of the fine and coarse components (d_s/d_L), lead to a lower minimum porosity [29]. Porosity results were determined by measuring the mass of particles in a known volume. Knowing the mass, the porosity can be calculated as follows:

$$\varepsilon = 1 - \frac{m_b}{m_s} = 1 - \frac{m_b}{\rho_s \cancel{V}} \tag{7}$$

where m_b is the bulk mass recorded by the scale and m_s is the mass that would occupy the known volume $\cancel{V}$ if it were non-porous. The non-porous mass can be calculated by knowing the absolute density of the particle and the volume occupied by the particles during the test. For this study, 50 ml of particles were poured into a 100 ml graduated cylinder, and the mass was taken with a Mettler Toledo XS403S scale. Five porosity measurements were taken for each particle system, and the average of the measurements was used as the porosity for that sample. Propagation of error was used to calculate the uncertainty for each measurement. Extra care was taken to ensure that the samples were well mixed when performing all porosity and thermal conductivity measurements.

2.3 Thermal Conductivity Measurement Methods

The TEMPOS Thermal Properties Analyzer, a hand-held needle probe that uses a transient line heat source method to measure the thermal conductivity, was used for all the monodisperse and binary particle systems at temperatures 25, 100, and 150 ℃. To make a measurement, the probe (TR-3 with diameter of 2.4 mm and length of 100 mm) was inserted into a 50.8 mm x 50.8 mm x 114.3 mm container of the particles being tested. The dimensions of the container were determined to ensure that at least 1.5 cm of material was parallel to the probe on all sides as per the recommendations of the user manual.

Because the TEMPOS Thermal Analyzer is limited to measuring thermal conductivity up to temperatures of 150 ℃, two particles samples were sent to Thermtest, a company that specializes in building thermal conductivity instrumentation and taking thermal conductivity measurements. The particle samples that were sent to Thermtest were CP 16/30 and the binary mixture CP 16/30 – CP 70/140 X_L=0.5. These samples were tested at temperatures of 100, 250, and 300 ℃ on the Thermtest Hot Disk TPS 2500 S, an instrument that uses a transient plane source (TPS) hot disk method in accordance with ISO22007-2.2. The sensor (Kapton tape sensor 5501 with diameter of 2.4 mm) is placed in a container with a volume of particles of 20 mm diameter and 20 mm height. Each packed bed sample was tested 10 times (for porosity and thermal conductivity with TEMPOS probe) and 3 times (Thermtest Hot Disk measurement). Samples were tapped lightly before measurements to provide some degree of settling to the packed beds. Particles were not removed from test chamber between subsequent tests as long heating times is required due to the sensor size. This is justified as large sensor sizes for both

instruments were used which minimize errors associated with contact resistance with the probes (noted in both instrument manuals). Error bars for thermal conductivity are based on the using the 95% confidence interval and the student's t-test and the ASME model for combining uncertainties[33]. Systematic error is based on 10% accuracy reported for the Tempos instrument and less than 5% reported for the Thermtest Hot Disk instrument. Additional uncertainty for the measurement (from standard deviation is included), as well as for the regression uncertainty reported in TEMPOS output. Error bar for porosity measurements utilize the student's t-value and standard deviation for 95% confidence interval.

3. Theory

3.1 Porosity Modeling

Generally, the porosity of a stagnant monodisperse particle bed ranges somewhere between 0.36-0.40 depending whether the system is loosely or densely packed [34]. This relationship has been shown to agree well with discrete element method simulations for particles with diameters between 100-1000 μm [28]; however, experimental measurements of potential granular media show a wider range of porosity values from 0.35-0.48 [22]. In current shell-and-plate moving packed bed heat exchanger models, it is have been common practice to use a porosity of either 0.40 or 0.45 [13,35]. Given that monodisperse particles have a small range of porosity values, there is an opportunity to decrease porosity by incorporating a binary particle system.

For modeling in this paper, each particle system will be considered as a monodisperse particle with a single size calculated using Sauter mean diameter. While the five standard CARBO ceramic particles are not strictly monodisperse, the particle size distributions are not wide enough to cause a large change in packed bed porosity because the size ratio between the major components of the particle systems are quite large (>0.70). The measured porosity shown in Section 4.1 supports this assumption because both the CP and HSP particle systems have porosities of 0.36 & 0.384, respectively. Using the packed bed porosity generated from the porosity model is acceptable because the thermal conductivity modele allows for the actual bed porosity to be used for polydisperse particle distribution instead of the distribution parameter in the original ZBS model proposed [27]. Two porosity models will be utilized here to determine the critical role of the porosity model on the effective packed bed thermal conductivity.

3.1.1 Yu and Standish Porosity Model

This study uses the empirical description of spherical particle binary mixtures developed by Yu & Standish [29]. This model shows how a conic equation can generally describe the relationship between the specific volume and the fractional solid volumes of binary mixtures. The model is described as follows:

$$\left(\frac{V-V_1X_1}{V_2}\right)^2+2G\left(\frac{V-V_1X_1}{V_2}\right)\left(\frac{V-X_1-V_2X_2}{V_1-1}\right)+\left(\frac{V-X_1-V_2X_2}{V_1-1}\right)^2=1 \tag{8}$$

where V is the specific volume of the binary packing, V_1 & V_2 are the partial specific volumes of the particles in the mixture, X_1 and X_2 are the solid volume fractions of the coarse and fine particles, respectively, and G is a parameter that is dependent on the initial specific volumes and size ratio. Please note that $V_1=V_2=(1-\varepsilon_o)^{-1}$, $X_1=1-X_2$, and

$$V=\frac{-B+\sqrt{B^2-4AC}}{2A} \tag{9}$$

where

$$A=\left(\frac{1}{V_2}\right)^2+\frac{2G}{V_2(V_1-1)}+\frac{1}{(V_1-1)^2} \tag{10}$$

$$B=-\frac{2V_1X_1}{(V_2)^2}+\frac{2G}{V_2(V_1-1)}(V_2X_1-V_2-X_1-V_1X_1)+\frac{2(V_2X_1-V_2-X_1)}{(V_1-1)^2} \tag{11}$$

$$C=-\left(\frac{V_1X_1}{V_2}\right)^2+\frac{2G}{V_2(V_1-1)}V_1X_1(V_2X_1-V_2-X_1)+\left(\frac{(V_2X_1-V_2-X_1)^2}{(V_1-1)^2}\right)^2-1 \tag{12}$$

G is the only unknown variable in equations 9-11. Luckily, G can be determined experimentally. Standish & Yu summarized experimental data from many binary mixture experiments and concluded that the maximum void contraction in packed bed porosity ($\Delta\varepsilon$) and large particle solid volume fraction leading to the largest porosity contraction (X_1^{max}) are functions of the initial monodisperse porosity (ε_0) and particle size ratio (r) [36]:

$$\Delta\varepsilon(r)=\begin{cases}\varepsilon_0(1-\varepsilon_0)(1-2.35r+1.35r^2) & r\le 0.741\\ 0 & r>0.741\end{cases} \tag{13}$$

$$X_1^{max}=\frac{1-r^2}{1+\varepsilon_0} \tag{14}$$

Assuming the binary mixtures experiences a maximum void contraction, the minimum specific volume of the binary mixture and the parameter G are calculated as follows:

$$V_{min} = \frac{1}{1 - \varepsilon_0 + \Delta\varepsilon(\mathrm{r})} \tag{15}$$

$$G = \frac{1 - \left(\frac{V_{min} - V_1 X_1^{max}}{V_2}\right)^2 - \left(\frac{V_{min} - V_2 - X_1^{max} + V_2 X_1^{max}}{V_1 - 1}\right)^2}{2\left(\frac{V_{min} - V_1 X_1^{max}}{V_2}\right)\left(\frac{V_{min} - V_2 - X_1^{max} + V_2 X_1^{max}}{V_1 - 1}\right)} \tag{16}$$

Once the parameter G is known, the specific volume of the binary mixture (Equation 7), and corresponding packed bed porosity can be calculated. Parametrically studying this model shows that lower particle size ratio will lead to a larger decrease in porosity for a given initial porosity. Similarly, a mixture with a lower initial porosity will have a lower porosity at the same size ratio as mixture with a higher initial porosity.

3.1.2 Deng and Chang Porosity Model

While the Yu and Standish porosity model provides a linear empirical model for porosity, Chang and Deng [37] recently proposed a non-linear packing model that demonstrated improved accuracy for multi-sized particle mixtures. In this procedure two potential porosity values are determined with the equations below:

$$\varepsilon^{(1)} = \varepsilon_1 X_1 + \left(\varepsilon_2 - a_2^{(1)}(1 + \varepsilon_2)\right) X_2 \tag{17}$$

$$\varepsilon^{(2)} = \left(\varepsilon_1 - b_1^{(2)}(\varepsilon_1)\right) X_1 + \varepsilon_2 X_2 \tag{18}$$

Where ε_1 and ε_2 are the porosities of the small and large particles respectively. The parameters *a* and *b* are found from the following:

$$a_j^{(i)} = \begin{cases} \left(1 - \frac{d_j}{d_i}\right)^p & for\ \ d_i > d_j \\ 0 & for\ \ d_j \geq d_i \end{cases} \tag{19}$$

$$b_j^{(i)} = \begin{cases} \left(1 - \frac{d_i}{d_j}\right)^s & for\ \ d_i < d_j \\ 0 & for\ \ d_i \geq d_j \end{cases} \tag{20}$$

Where d_i and d_j are the particle diameters of the ith and jth particles respectively; p and s are empirically determined constants. Parameters *p* and *s* can be determined empirically by measured values of the porosity at different size ratios and large particle volume fraction, details

of this procedure can be found in the appendix of Chang and Deng [37]. Once the two potential porosity values are found from equations 17 and 18 the porosity of the mixture can be found as the maximum porosity of the values obtained for each class of particles:

$$\varepsilon = max\left(\varepsilon^{(1)}, \varepsilon^{(2)}\right) \tag{21}$$

The two porosity models are used in conjunction with a well-established correlation regarding packed bed thermal conductivity. Table 3 provides details on the fitting parameters found using the Chang and Deng model for both HSP and CP particle types.

3.2 Thermal Conductivity Modeling

Similar to porosity, two conductivity models are investigated to understand the predictive capacity of effective thermal conductivity of packed beds of particles.

3.2.1 Zehner, Bauer, and Schlünder Model (ZBS Model)

The Zehner, Bauer, and Schlünder Model (ZBS Model) is used in this paper to calculate the effective packed bed thermal conductivity [23]. The ZBS model is a well-respected effective bulk thermal conductivity model that has been used in numerous studies [13,22,38–40]. Current shell-and-plate moving packed bed heat exchanger literature applies the ZBS Model with monodisperse particles at a constant porosity [3,13]. While this approach is great for understanding trends associated with particle size, this study will explore how binary particle systems with bimodal size distributions decrease packed bed porosity and increase effective thermal conductivity. According to Tsotsas & Schlünder, there is precedent for using the ZBS model with a wide particle size distribution as long as the Sauter mean diameter (Equation 6) and the actual packed bed porosity are used in the calculations [27].

The ZBS model is dependent on many different parameters including packed bed porosity (ε), packed bed temperature (T), particle diameter (d_p), particle emissivity (ε_r), an empirical particle contact parameter (φ), the solid particle thermal conductivity (k_s), gas thermal conductivity (k_f), and gas pressure (P). Table 3 outlines all the parameters and associated references that are used in this study. The initial porosity of the five non-binary particle systems was calculated by averaging the porosity measurements for the two particle types used in this study. The average porosity of the CP and HSP particle systems were 0.36 & 0.384, respectively.

These initial porosity values are acceptable for this study because they fall between the accepted porosity values for loose and dense packed spheres of 0.40 and 0.36, respectively [34]. The model equations will not be described in this article for brevity, but interested researchers can read van Antwerpen's review for a good description of the ZBS model and other packed bed thermal conductivity models [24]. The only modification to the original ZBS model used in this study is the deformation parameter provided by Hso et al. because it was found to be more accurate [41].

$$B = 1.364\left(\frac{1-\varepsilon}{\varepsilon}\right)^{1.055} \tag{21}$$

Table 4 shows the specific assumptions made while using the ZBS model.

3.2.2 Yagi and Kunii Model

The ZBS model is widely utilized for modeling effective thermal conductivity in moving packed beds and energy storage applications but as noted in Antwerpen et al. other correlations exist [24]. An additional model that is commonly used for high temperature particle beds is that of Yagi and Kunii [42]. This model has been used for catalytic packed bed reactors of methanol [43], heat transfer in ash deposits of utility boilers [44], pyrolysis fixed bed reactors[40], and in moving packed bed particle-to-sCO_2 heat exchangers [14,15]. The Yagi and Kunii model establishes the effective thermal conductivity as:

$$k_{s,eff} = \frac{k_f \beta(1-\varepsilon)}{\gamma\frac{k_f}{k_s}+\phi} \tag{22}$$

where β, and γ are constants from Yagi and Kunii (set as 1 for most models and used here)[42]. The parameter ϕ can be found from:

$$\phi = \frac{1}{4}\left(\frac{\{(K-1)/K\}^2}{\ln K-(K-1)/K}\right) - \frac{1}{3K} \tag{23}$$

Where K is the ratio of the particle to the gas phase thermal conductivity[18]. Notably this model lacks a temperature dependent component relative to the ZBS model. While

modifications have been developed to include radiative effects, these are neglected for fine particles, which is relevant here with the binary particle sizes [14].

4. Results and Discussion

4.1 Porosity Model Results

Figure 2 shows how large particle volume fraction changes the mixture composition for HSP 16/30 – HSP 40/70. The difference between near wall packing of the coarse HSP 16/30 and the fine HSP 40/70 is evident. While HSP 40/70 appears to have the best contact with the near-wall, there is reason to believe that using a mixture of coarse and fine particles could improve heat transfer by increasing bulk thermal conductivity while also keeping near-wall contact resistance low [45].

Figure 3A shows the theoretical Standish & Yu model porosity as a function of large particle volume fraction for each of the binary particle systems tested in this study. The porosity for each particle mixture initially experiences a decrease in porosity as the large particle volume fraction increases until reaching a minimum porosity value where the porosity then increases to that of a monodisperse particle system. Figure 3B-D shows the experimental porosity results for HSP 16/30 – HSP 40/70, CP 16/30 – CP 40/100, and CP 16/30 – CP 70/140 in comparison to the theoretical model. As expected, the mixture experiences a decrease in porosity from the introduction of a bimodal particle distribution; however, the decrease in porosity is not as pronounced as expected. There a few explanations for the deviation in the results. First, the particle distributions are not strictly binary, instead the distributions are bimodal. This paper approximates each CARBO particle system (e.g. HSP 16/30) as a monodisperse particle with the Sauter mean diameter calculated from each particle distribution. This could impact the porosity measurements; however, the size distribution for each CARBO particle is narrow, so the impact of this on the measurement should be minor. Secondly, due to the complexity of real-life particle packing, it is very difficult to create a model that accurately captures all packing mechanisms. Theoretical correlations for particle packing have been known to overestimate the contraction in porosity, especially when $0.5 < X_L < 0.75$ [37,46]. Because of this limitation the Chang and Deng model for porosity was also applied.

Figure 4A shows the predicted porosity for the samples tested using the Chang and Deng model for porosity. Notably, the shape of these models is substantially different than the Standish and Yu model and the decrease in porosity predicted is smaller. Figures 4B-D shows

the theoretical model of Chang and Deng in comparison to the measured porosity. As can be seen the Chang and Deng model does provide a better prediction for the vast majority of the particles, with the exception of the CP 16/30 – CP 40/100 mixture.

Table 5 summarizes the two models and the experimental results for the porosity. As can be seen the Chang and Deng provides a better estimate of the porosity across the range of measured values tested here. Of particular note is the better prediction accuracy within the $0.5 < X_L < 0.75$ range, with only minimal improvements, and in some cases decreased performance, outside of this range. The average % difference between the model and experiment is 10% for the Standish and Yu and 4.1% for the Chang and Deng model further indicating the improved model capability for predicting the porosity of the mixture. While this is an important conclusion, the focus remains on the impact to the packed bed thermal conductivity and

determining if the predictive models can be applied within the ZBS correlation.

4.2 Thermal Conductivity

In the previous section two different porosity modeling approaches were investigated, and the results indicated that the Chang and Deng model provided more accurate results over the widest range of particle size ratios and large particle volume fractions tested. While this result is relevant, understanding the ultimate impact on the effective packed bed thermal conductivity is critical and both models were investigated. Figures 5A and 5B are comparisons of the predicted changes in porosity and effective thermal conductivity at 100 ℃ for both the Standish and Yu and Chang and Deng models respectively. The models show that smaller particle size ratios lead to a lower minimum porosity and higher maximum thermal conductivity. Additionally, the Chang and Deng porosity model results in smaller overall changes in effective thermal conductivity, due to the smaller impact on the overall porosity. For the CP 16/30 – CP 70/140 mixture this results in a maximum percent increase in effective thermal conductivity relative to the large particle only of 42% and 27% for Standish and Yu and Chang and Deng models respectively.

Figure 6 shows the results for both HSP and CP particle systems for temperatures up to 150°C. As can be seen the ZBS model in combination with the Chang and Deng porosity model tends to underpredict the packed bed effective thermal conductivity particularly for smaller size ratios, and in general provides only a moderate degree of prediction accuracy. The experimental results do show that substantial increases in packed bed thermal conductivity can be achieved

through this simple approach of mixing two distinct particle sizes together. The data is further expanded for all of the CP particles in Table 6 (and for all the particles in the appendix). Overall, from these results the ZBS model using the Chang and Deng porosity model only provides a slightly improved prediction accuracy (14% error compared to 15% error for Standish and Yu). Considering the much-improved prediction accuracy of the porosity measurement, it would be expected to see larger gains in the prediction accuracy for the packed bed thermal conductivity. This could potentially indicate limitations with the ZBS model in predicting the effective packed bed thermal conductivity of binary particle systems.

In addition to the temperatures reported in Figure 6, the ZBS model is compared with experimental results for CP 16/30 - CP 70/140 250, and 300 ℃ in Figure 7 (notably these are the first experiments to our knowledge of effective packed bed thermal conductivity of binary particle mixtures at these temperature levels). As can be seen in Figures 7A-B and 7C-D the ZBS model with both porosity models tends to underpredict the effective packed bed thermal conductivity of the measured samples, with a more dramatic underprediction from the use of the Chang and Deng model. This is particularly challenging as the Chang and Deng model has been shown to provide a better prediction of the packed bed porosity, but there is a clear disconnect when applied in the existing ZBS model that can't currently be reconciled with the data collected here.

Figure 8 presents the same results as Figure 6 but with respect to the Yagi and Kunii model for thermal conductivity, only the Chang and Deng is utilized for porosity based on the improved predictive capacity already demonstrated. Notably, the Yagi and Kunii model for effective thermal conductivity consistently overpredicts at low temperatures and does not capture the significant changes that occur as a function of changing porosity. Similar to the results with the ZBS model, inspection of the results in Figure 8 demonstrate that the Yagi and Kunii model is also not predictive for a binary particle system and more understanding is needed.

While the results presented above clearly show some limitations of utilizing the ZBS and the Yagi and Kunii effective thermal conductivity models, the ZBS model provides a reasonable conservative estimate for packed bed effective thermal conductivity.

5. Conclusions & Future Work

This work contributes to the field particles as heat transfer fluids and particle-based energy storage by exploring how packed bed thermal conductivity could be increased in particle-based applications such as moving packed bed heat exchangers and particle-based energy storage

simply by mixing two particles together. This is unique to previous studies because others have not considered using bimodal particle size distributions in moving packed bed heat exchangers. Five ceramic particles with sizes between 100 - 1000 μm were selected to make nine unique binary particle systems to investigate the impact on porosity and effective thermal conductivity. The Standish and Yu and Chang and Deng models for porosity were investigated with significantly better prediction capability provided by the Chang and Deng porosity model. While the Chang and Deng porosity model provided a better prediction of porosity, both porosity models when used in conjunction with the ZBS model for effective thermal conductivity resulted in underpredicting the effective thermal conductivity. Utilization of the Chang and Deng porosity model with the Yagi and Kunii thermal conductivity model did not result in improved prediction of thermal conductivity of the packed bed for the binary particle system either. Further work is needed to understand this discrepancy at the temperatures studied here, as well as further experiments at higher temperatures. As a result, this study demonstrates that binary particle systems should be considered as a potential option for improving effective thermal conductive of packed particle beds but further work is needed: higher temperature studies, and understanding how flowing packed bed porosity will change for the binary particle system. While bulk porosity for a stagnant packed bed is shown to decrease, more work should be done to show that the moving packed bed porosity is decreased. Because smaller particles have been shown in multiple studies to be the biggest factor in increasing the overall heat transfer coefficient [13,45,47], it will be important to study if a decrease in bulk and near-wall porosity from using a particle size distribution can outperform current single particle systems. Further work could also focus on the role of changing particle packing between subsequent measurements, although this variation is expected to be minor based on the probe size chosen here.

While this study demonstrates that smaller size ratios lead to a greater decrease in porosity, future research should focus on what size ratio can be used in a practical system due to the risk of particle segregation for small size ratio mixtures. Future studies should also consider the flowability of particle systems with wide size distribution, especially at higher temperatures. Additionally, further studies should focus on experimental measurements of effective thermal conductivity at increased operating temperatures more likely to be seen in advanced power cycles (i.e. > 500°C). Other than improving thermal conductivity, binary particle systems could potentially reduce near-wall particle resistance by having a smaller effective particle size. This

could result in an increase in the overall heat transfer coefficient of particle-to-sCO_2 heat exchangers at little to no additional capital investment. While the work here focused on impact to effective thermal conductivity another interesting aspect for future investigation could focus on the heat storage density as the reduction in the porosity would increase the overall storage volume per unit volume of container.

Acknowledgements

The authors would like to acknowledge partial support of this work from the U.S. Department of Energy Solar Energy Technologies Office under award number DE-EE0009375

References

[1] ARPA-E, Duration Addition to electricitY Storage (DAYS) Overview, Dep. Energy. (2018) 1–12.

[2] M. Mehos, C. Turchi, J. Vidal, M. Wagner, Z. Ma, C. Ho, W. Kolb, C. Andraka, M. Mehos, C. Turchi, J. Vidal, M. Wagner, Z. Ma, C. Ho, W. Kolb, C. Andraka, A. Kruizenga, NREL, Concentrating Solar Power Gen3 Demonstration Roadmap, 2017. https://doi.org/10.2172/1338899.

[3] C.K. Ho, M. Carlson, K.J. Albrecht, Z. Ma, S. Jeter, C.M. Nguyen, Evaluation of Alternative Designs for a High Temperature Particle-to-sCO2 Heat Exchanger, J. Sol. Energy Eng. 141 (2019) 1–9. https://doi.org/10.1115/1.4042225.

[4] A. Calderón, C. Barreneche, A. Palacios, M. Segarra, C. Prieto, A. Rodriguez-Sanchez, A.I. Fernández, Review of solid particle materials for heat transfer fluid and thermal energy storage in solar thermal power plants, Energy Storage. 1 (2019) 1–20. https://doi.org/10.1002/est2.63.

[5] A. Calderón, A. Palacios, C. Barreneche, M. Segarra, C. Prieto, A. Rodriguez-Sanchez, A.I. Fernández, High temperature systems using solid particles as TES and HTF material: A review, Appl. Energy. 213 (2018) 100–111. https://doi.org/10.1016/j.apenergy.2017.12.107.

[6] J. Gifford, Z. Ma, P. Davenport, Thermal Analysis of Insulation Design for a Thermal Energy Storage Silo Containment for Long-Duration Electricity Storage, Front. Energy Res. 8 (2020) 1–12. https://doi.org/10.3389/fenrg.2020.00099.

[7] Department of Energy, DOE Pursues SunShot Initiative to Achieve Cost Competitive Solar Energy by 2020, Dep. Energy. (2011).

[8] K.J. Albrecht, C.K. Ho, High-temperature flow testing and heat transfer for a moving packed-bed particle/sCO2 heat exchanger, AIP Conf. Proc. 2033 (2018). https://doi.org/10.1063/1.5067039.

[9] K.J. Albrecht, M.D. Carlson, H.F. Laubscher, R. Crandell, N. DeLovato, C.K. Ho, Testing and model validation of a prototype moving packed-bed particle-to-sCO2 heat exchanger, Proc. 7Th Int. Conf. Electron. Devices, Syst. Appl. 2306 (2020) 030002. https://doi.org/10.1063/5.0031483.

[10] G. Zanganeh, A. Pedretti, A. Haselbacher, A. Steinfeld, Design of packed bed thermal energy storage systems for high-temperature industrial process heat, Appl. Energy. 137 (2015) 812–822. https://doi.org/10.1016/j.apenergy.2014.07.110.

[11] M. Sedighi, R. Vasquez Padilla, R.A. Taylor, Efficiency limits of high-temperature transparent packed-bed solar receivers, Energy Convers. Manag. 241 (2021) 114257. https://doi.org/10.1016/j.enconman.2021.114257.

[12] S. Trevisan, W. Wang, B. Laumert, Coatings utilization to modify the effective properties of high temperature packed bed thermal energy storage, Appl. Therm. Eng. 185 (2021) 116414. https://doi.org/10.1016/j.applthermaleng.2020.116414.

[13] K.J. Albrecht, C.K. Ho, Design and operating considerations for a shell-and-plate, moving packed-bed, particle-to-sCO 2 heat exchanger, Sol. Energy. 178 (2019) 331–340. https://doi.org/10.1016/j.solener.2018.11.065.

[14] J. Yin, Q. Zheng, X. Zhang, Heat transfer model of a particle energy storage-based moving packed bed heat exchanger, Energy Storage. 2 (2020) 1–14. https://doi.org/10.1002/est2.113.

[15] K.J. Albrecht, C.K. Ho, Heat Transfer Models of Moving Packed-Bed Particle-to-sCO2 Heat Exchangers, J. Sol. Energy Eng. 141 (2019) 1–8. https://doi.org/10.1115/1.4041546.

[16] V. Gnielinski, New Equations for Heat and Mass Transfer in Turbulent Pipe and Channel Flow, Int. Chem. Eng. 16 (1976) 359–367.

[17] Y.S. Muzychka, E. Walsh, P. Walsh, Simple models for laminar thermally developing

slug flow in non-circular ducts and channels, ASME Int. Mech. Eng. Congr. Expo. Proc. 9 (2010) 1867–1878. https://doi.org/10.1115/IMECE2009-10484.

[18] A. Denloye, J. Botterill, A Theoretical Model of Heat Transfer to a packed or quiescent fluidized bed, Chem. Eng. Sci. 33 (1978) 509–515.

[19] T.K. Chu, C.Y. Ho, Thermal Conductivity and Electrical Resistivity of Eight Selected AISI Stainless Steels, in: Therm. Conduct. 15, Springer US, Boston, MA, 1978: pp. 79–104. https://doi.org/10.1007/978-1-4615-9083-5_12.

[20] R. Span, W. Wagner, A New Equation of State for Carbon Dioxide Covering the Fluid Region from the Triple-Point Temperature to 1100 K at Pressures up to 800 MPa, J. Phys. Chem. Ref. Data. 25 (1996) 1509–1596. https://doi.org/10.1063/1.555991.

[21] V. Vesovic, W.A. Wakeham, G.A. Olchowy, J. V. Sengers, J.T.R. Watson, J. Millat, The Transport Properties of Carbon Dioxide, J. Phys. Chem. Ref. Data. 19 (1990) 763–808. https://doi.org/10.1063/1.555875.

[22] T. Baumann, S. Zunft, Properties of granular materials as heat transfer and storage medium in CSP application, Sol. Energy Mater. Sol. Cells. 143 (2015) 38–47. https://doi.org/10.1016/j.solmat.2015.06.037.

[23] R. Bauer, E.U. Schlünder, Effective radial thermal conductivity of packings in gas flow. Part II. Thermal conductivity of the packing fraction without gas flow, Int. Chem. Eng. 18 (1978) 189–204.

[24] W. Van Antwerpen, C.G. Du Toit, P.G. Rousseau, A review of correlations to model the packing structure and effective thermal conductivity in packed beds of mono-sized spherical particles, Nucl. Eng. Des. 240 (2010) 1803–1818. https://doi.org/10.1016/j.nucengdes.2010.03.009.

[25] M. Díaz-Heras, J.F. Belmonte, J.A. Almendros-Ibáñez, Effective thermal conductivities in packed beds: Review of correlations and its influence on system performance, Appl. Therm. Eng. 171 (2020) 115048. https://doi.org/10.1016/j.applthermaleng.2020.115048.

[26] N.P. Siegel, M.D. Gross, R. Coury, The Development of Direct Absorption and Storage Media for Falling Particle Solar Central Receivers, J. Sol. Energy Eng. 137 (2015) 041003. https://doi.org/10.1115/1.4030069.

[27] E. Tsotsas, E.-U. Schlünder, Impact of particle size dispersity on thermal conductivity of packed beds: Measurement, numerical simulation, prediction, Chem. Eng. Technol. 14 (1991) 421–427. https://doi.org/10.1002/ceat.270140610.

[28] R.Y. Yang, R.P. Zou, A.B. Yu, D. Waals, Computer simulation of the packing of fine particles, 62 (2000) 3900–3908.

[29] A.B. Yu, N. Standish, An analytical—parametric theory of the random packing of particles, Powder Technol. 55 (1988) 171–186. https://doi.org/10.1016/0032-5910(88)80101-3.

[30] N. Siegel, G. Kolb, Design and on-sun testing of a solid particle receiver prototype, 2008 Proc. 2nd Int. Conf. Energy Sustain. ES 2008. 2 (2009) 329–334. https://doi.org/https://doi.org/10.1115/ES2008-54090.

[31] CARBO, CARBOBEAD Technical Data Sheet, (2019) 1–2.

[32] M. V. Bagepalli, J.D. Yarrington, A.J. Schrader, Z.M. Zhang, D. Ranjan, P.G. Loutzenhiser, Measurement of flow properties coupled to experimental and numerical analyses of dense, granular flows for solar thermal energy storage, Sol. Energy. 207 (2020) 77–90. https://doi.org/10.1016/j.solener.2020.06.062.

[33] R.H. Dieck, Measurement Uncertainty: Methods and Applications, 5th ed., International Society of Automation, Research Triangle Park, NC, 2017.

[34] R.K. McGEARY, Mechanical Packing of Spherical Particles, J. Am. Ceram. Soc. 44 (1961) 513–522. https://doi.org/10.1111/j.1151-2916.1961.tb13716.x.

[35] K.J. Albrecht, C.K. Ho, Heat Transfer Models of Moving Packed-Bed Particle-to-sCO2 Heat Exchangers, J. Sol. Energy Eng. Trans. ASME. 141 (2017) 1–10.

https://doi.org/10.1115/1.4041546.

[36] A.B. Yu, N. Standish, Porosity calculations of multi-component mixtures of spherical particles, Powder Technol. 52 (1987) 233–241. https://doi.org/10.1016/0032-5910(87)80110-9.

[37] C.S. Chang, Y. Deng, A nonlinear packing model for multi-sized particle mixtures, Powder Technol. 336 (2018) 449–464. https://doi.org/10.1016/j.powtec.2018.06.008.

[38] Z. Peng, E. Doroodchi, B. Moghtaderi, Heat transfer modelling in Discrete Element Method (DEM)-based simulations of thermal processes: Theory and model development, Prog. Energy Combust. Sci. 79 (2020) 100847. https://doi.org/10.1016/j.pecs.2020.100847.

[39] M. Moscardini, Y. Gan, S. Pupeschi, M. Kamlah, Discrete element method for effective thermal conductivity of packed pebbles accounting for the Smoluchowski effect, Fusion Eng. Des. 127 (2018) 192–201. https://doi.org/10.1016/j.fusengdes.2018.01.013.

[40] Y. Qian, Z. Han, J.-H. Zhan, X. Liu, G. Xu, Comparative evaluation of heat conduction and radiation models for CFD simulation of heat transfer in packed beds, Int. J. Heat Mass Transf. 127 (2018) 573–584. https://doi.org/10.1016/j.ijheatmasstransfer.2018.06.127.

[41] C.T. Hsu, P. Cheng, K.W. Hong, Modified Zehner-Schlunder Models for Stagnant Thermal Conductivity of Porous Media, Int. J. Heat Mass Transf. 37 (1994) 2751–2759.

[42] S. Yagi, D. Kunii, Studies on effective thermal conductivities in packed beds, AIChE J. 3 (1957) 373–381. https://doi.org/10.1002/aic.690030317.

[43] A. Karim, J. Bravo, A. Datye, Nonisothermality in packed bed reactors for steam reforming of methanol, Appl. Catal. A Gen. 282 (2005) 101–109. https://doi.org/10.1016/j.apcata.2004.12.006.

[44] A. Zbogar, F.J. Frandsen, P.A. Jensen, P. Glarborg, Heat transfer in ash deposits: A modelling tool-box, Prog. Energy Combust. Sci. 31 (2005) 371–421. https://doi.org/10.1016/j.pecs.2005.08.002.

[45] A.O.O. Denloye, J.S.M. Botterill, Heat transfer in flowing packed beds, Chem. Eng. Sci. 32 (1977) 461–465. https://doi.org/10.1016/0009-2509(77)87001-2.

[46] S. Liu, Z. Ha, Prediction of random packing limit for multimodal particle mixtures, Powder Technol. 126 (2002) 283–296. https://doi.org/10.1016/S0032-5910(02)00075-X.

[47] M.C. Golob, Convective Heat Transfer Performance of Sand for Thermal Energy Storage, 2011.

[48] J.P. Holman, Heat Transfer, 10th ed., McGaw-Hill, New York, 2010.

Table 1. Sensitivity of packed bed thermal conductivity using the ZBS model for a monodisperse packed bed. For each evaluation, all standard parameters are used except for the parameter being modified.

Standard Properties	Value	Units	Sensitivity Study	
			Modified Parameter	% Change k_{eff}
Temperature	500	℃	Temperature (+10%)	4.43
Particle Diameter	500	μm	Particle Diameter (+10%)	1.29
Emissivity	0.9	~	Emissivity (+10%)	1.96
Particle Thermal Conductivity	2	W $m^{-1} K^{-1}$	Particle Thermal Conductivity (+10%)	3.45
Porosity	0.4	~	Porosity (-10%)	9.58

Table 2. Particles tested in this study. Particle properties can be seen in the CARBO data sheet [31] with the exception of the measured particle diameter.

Material	Sauter Mean Diameter [μm]	Measured Average Diameter [μm]	Particle Density, ρ_s [g cm^{-3}]	Size Ratio, *r* [-]
HSP 16/30	977	865 ±111	3.61	N/A
HSP 40/70	297	320 ±41.8		N/A
CP 16/30	937	1005 ±125	3.27	N/A
CP 40/100	262	186 ±32.2		N/A
CP 70/140	147	109 ±16.7		N/A
HSP 16/30 – HSP 40/70, X_L = 0.25	359	N/A	3.61	0.304
HSP 16/30 – HSP 40/70, X_L = 0.50	455			
HSP 16/30 – HSP 40/70, X_L = 0.611	517			
HSP 16/30 – HSP 40/70, X_L = 0.75	621			
CP 16/30 – CP 40/100, X_L = 0.25	319	N/A	3.27	0.279
CP 16/30 – CP 40/100, X_L = 0.50	409			
CP 16/30 – CP 40/100, X_L = 0.620	473			
CP 16/30 – CP 40/100, X_L = 0.75	569			
CP 16/30 – CP 70/140, X_L = 0.25	186	N/A	3.27	0.157
CP 16/30 – CP 70/140, X_L = 0.50	254			
CP 16/30 – CP 70/140, X_L = 0.665	336			
CP 16/30 – CP 70/140, X_L = 0.75	400			

Table 3. Fitting parameters used in the Chang and Deng Model for the particles tested in this study.

Particle Type	d_1 [μm]	d_2 [μm]	e_1	e_2	*a*	*b*	*p*	*s*
HSP	866	321	0.386	0.382	0.0579	0.2487	6.15	3
CP	1005	186	0.356	0.354	-0.120	0.116	17.49	5.71
	1005	109	0.356	0.37	-0.144	0.178		

Table 4. Parameters and assumptions for ZBS thermal conductivity modeling.

Parameter	**Value**	**Units**	**Ref.**
Particle Diameter (d_p)	See Table 2	μm	-
Initial Porosity (ε_0)	See Table 4	-	-
Particle Emissivity (ε_r)	0.9	-	[26]

Empirical Particle Contact (φ)	0.01	-	[24]
Particle Thermal Conductivity (k_s)	2.0	W m^{-1} K^{-1}	[3]
Gas Thermal Conductivity (k_f)	Air(T)	W m^{-1} K^{-1}	[48]
Pressure (P)	101.325	kPa	-

Table 5. Summary of modeled (S-Y:Standish and Yu, C-D: Chang and Deng) and experimentally measured porosities.

Material	ε_{S-Y}	ε_{C-D}	$\varepsilon_{experimental}$	% Difference S-Y	% Difference C-D
HSP 40/70	0.384	0.386	0.382	0.52%	1.05%
HSP 16/30 – HSP 40/70, X_L =0.25	0.343	0.366	0.352	2.56%	3.97%
HSP 16/30 – HSP 40/70, X_L = 0.50	0.312	0.346	0.34	8.24%	1.75%
HSP 16/30 – HSP 40/70, X_L = 0.75	0.322	0.359	0.35	8.00%	2.60%
HSP 16/30	0.384	0.382	0.386	0.52%	1.04%
CP 40/100	0.36	0.356	0.354	1.69%	0.56%
CP 16/30 – CP 40/100, X_L = 0.25	0.302	0.345	0.313	3.51%	10.34%
CP 16/30 – CP 40/100, X_L = 0.50	0.204	0.335	0.296	31.08%	13.09%
CP 16/30 – CP 40/100, X_L = 0.75	0.229	0.329	0.318	27.99%	3.34%
CP 16/30	0.36	0.354	0.356	1.12%	0.56%
CP 70/140	0.36	0.356	0.37	2.70%	3.78%
CP 16/30 – CP 70/140, X_L = 0.25	0.299	0.304	0.318	5.97%	4.30%
CP 16/30 – CP 70/140, X_L = 0.50	0.227	0.269	0.284	20.07%	5.15%
CP 16/30 – CP 70/140, X_L = 0.75	0.193	0.320	0.301	35.88%	6.21%
CP 16/30	0.36	0.370	0.356	1.12%	3.93%

Table 6. Thermal conductivity results for CP 16/30 – CP 40/100 for each temperature and particle system (* denotes measurement made with TPS 2500S system).

Material	Temperature (°C)	$k_{eff,S-Y}$ [W m^{-1}K^{-1}]	$k_{eff,C-D}$ [W m^{-1}K^{-1}]	$k_{eff,experiment}$ [W m^{-1}K^{-1}]	% Difference S-Y	% Difference C-D
CP 70/140	25	0.262	0.265	0.197	32.99%	34.46%
CP 16/30 – CP 70/140, X_L = 0.25		0.321	0.315	0.255	25.88%	23.68%
CP 16/30 – CP 70/140, X_L = 0.50		0.415	0.359	0.345	20.29%	4.15%
CP 16/30 – CP 70/140, X_L = 0.75		0.48	0.312	0.341	40.76%	8.50%
CP 16/30		0.284	0.275	0.235	20.85%	17.08%
CP 70/140	100	0.281	0.284	0.214	31.31%	32.66%
CP 16/30 – CP 70/140, X_L = 0.25		0.344	0.338	0.325	5.85%	3.91%
CP 16/30 – CP 70/140, X_L = 0.50*		0.443	0.385	0.446	0.67%	13.65%
CP 16/30 – CP 70/140, X_L = 0.50		0.443	0.385	0.399	11.03%	3.48%
CP 16/30 – CP 70/140, X_L = 0.75		0.513	0.338	0.406	26.35%	16.83%
CP 16/30*		0.312	0.303	0.34	8.24%	10.92%
CP 16/30		0.312	0.303	0.283	10.25%	7.02%
CP 70/140	150	0.292	0.296	0.257	13.62%	15.01%
CP 16/30 – CP 70/140, X_L = 0.25		0.358	0.351	0.361	0.83%	2.65%
CP 16/30 – CP 70/140, X_L = 0.50		0.46	0.401	0.394	16.75%	1.79%
CP 16/30 – CP 70/140, X_L = 0.75		0.534	0.354	0.492	8.54%	28.05%
CP 16/30		0.331	0.322	0.312	6.09%	3.09%
CP 16/30 – CP 70/140, X_L = 0.50*	250	0.491	0.431	0.531	7.53%	18.92%
CP 16/30*		0.37	0.360	0.426	13.15%	15.38%
CP 16/30 – CP 70/140, X_L = 0.50*	300	0.506	0.444	0.533	5.07%	16.64%
CP 16/30*		0.39	0.381	0.454	14.10%	16.12%

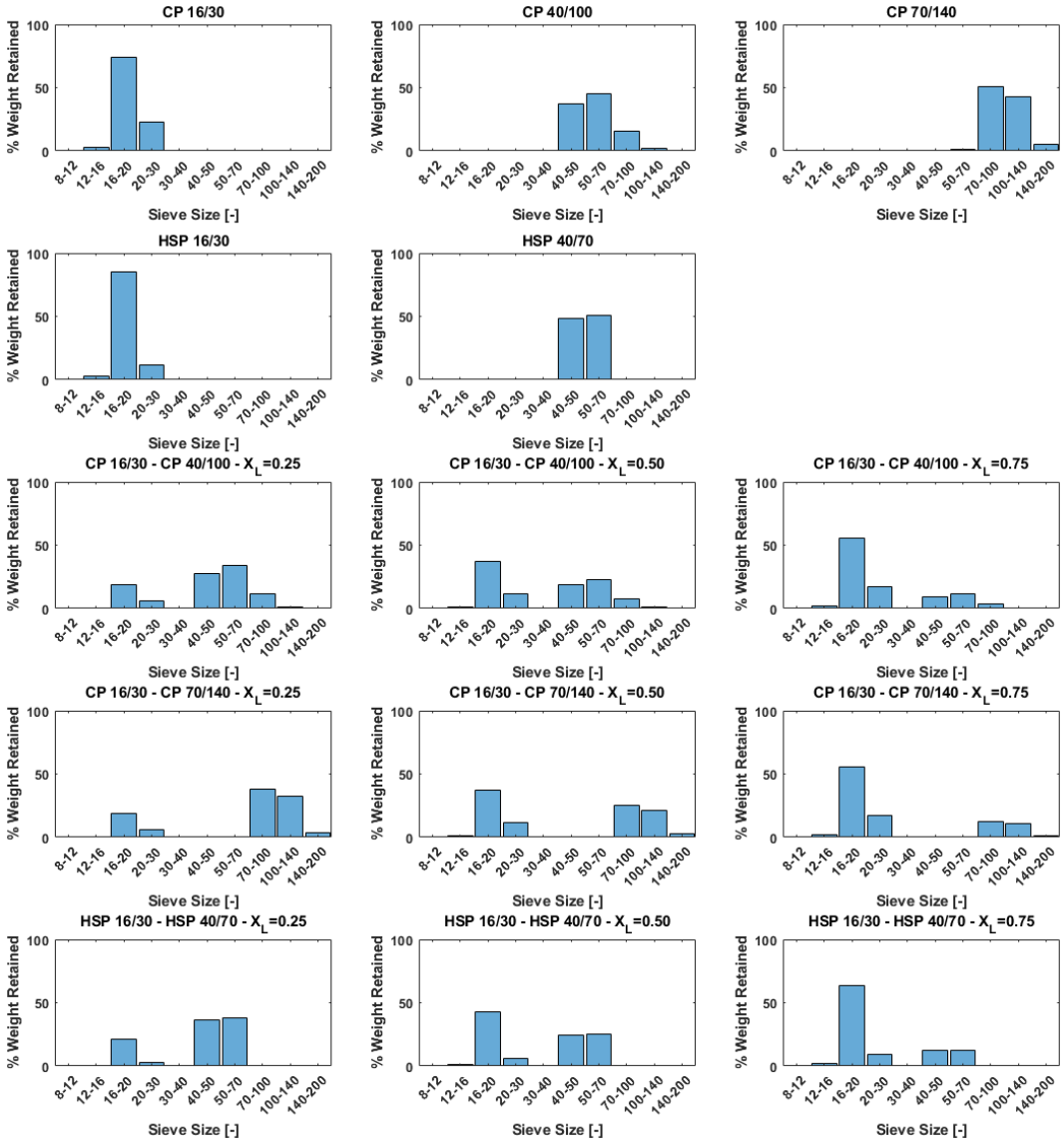

Figure 1. The particle size distributions for each particle sample tested. Data for the particle size distributions were either provided by CARBO with the particles or taken from the company's data sheet [31].

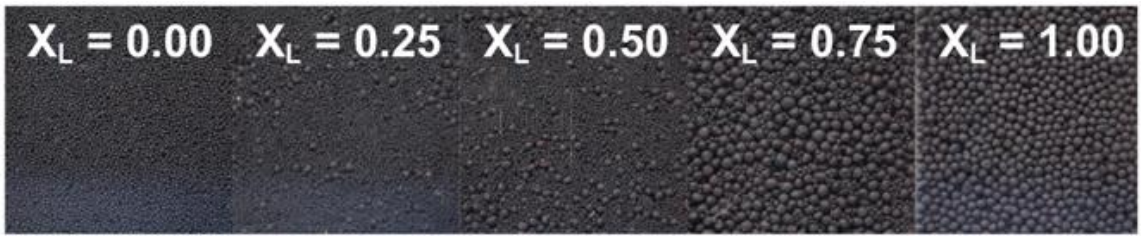

Figure 2. A) Particle mixtures of HSP 16/30 - HSP 40/70 used in this study. Each image is approximately 20mm x 20mm.

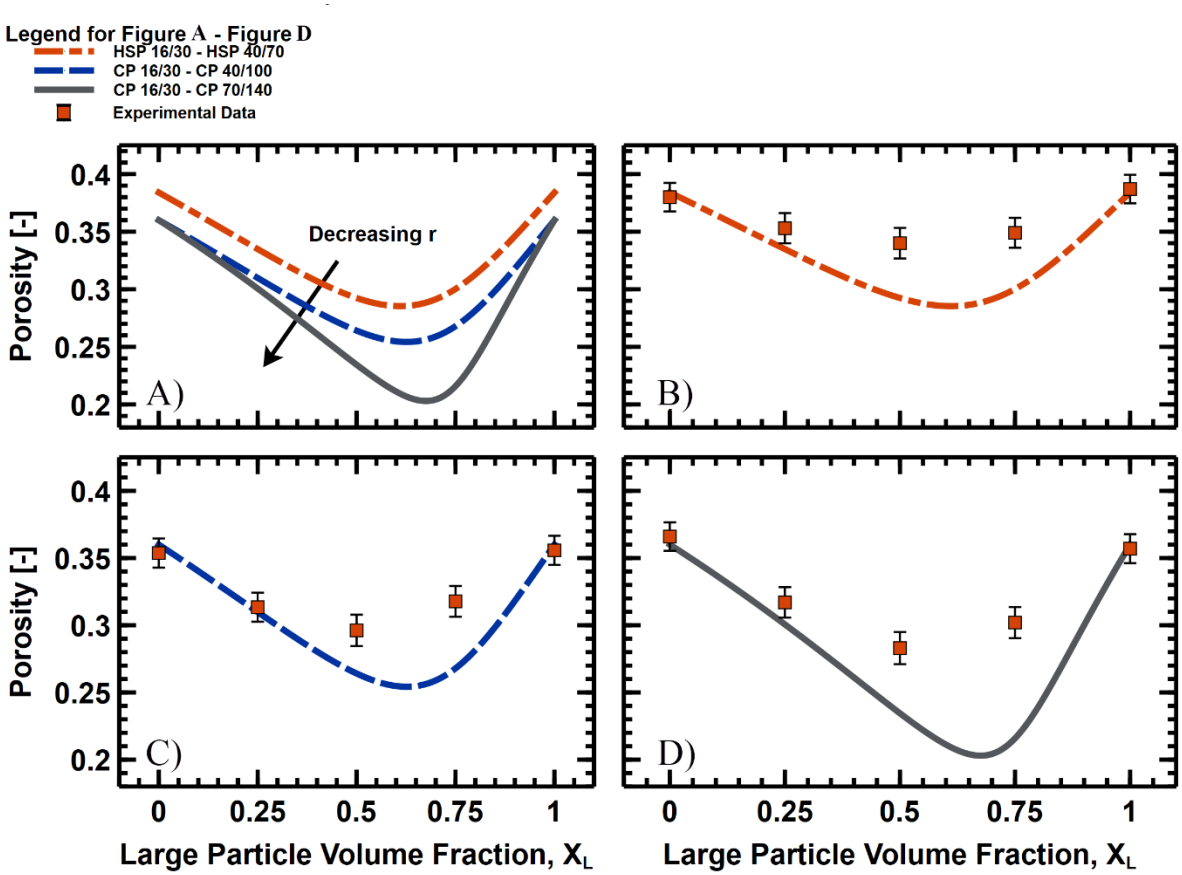

Figure 3. Comparison of theoretical (using the Standish and Yu model) and measured particle porosity: A) Standish and Yu Theoretical porosity as a function on large particle volume fraction for each of the binary particle systems tested. B-D) Porosity as a function of large particle volume fraction for HSP 16/30 – HSP 40/70, CP 16/30 – CP 40/100, and CP 16/30 – CP 70/140, respectively.

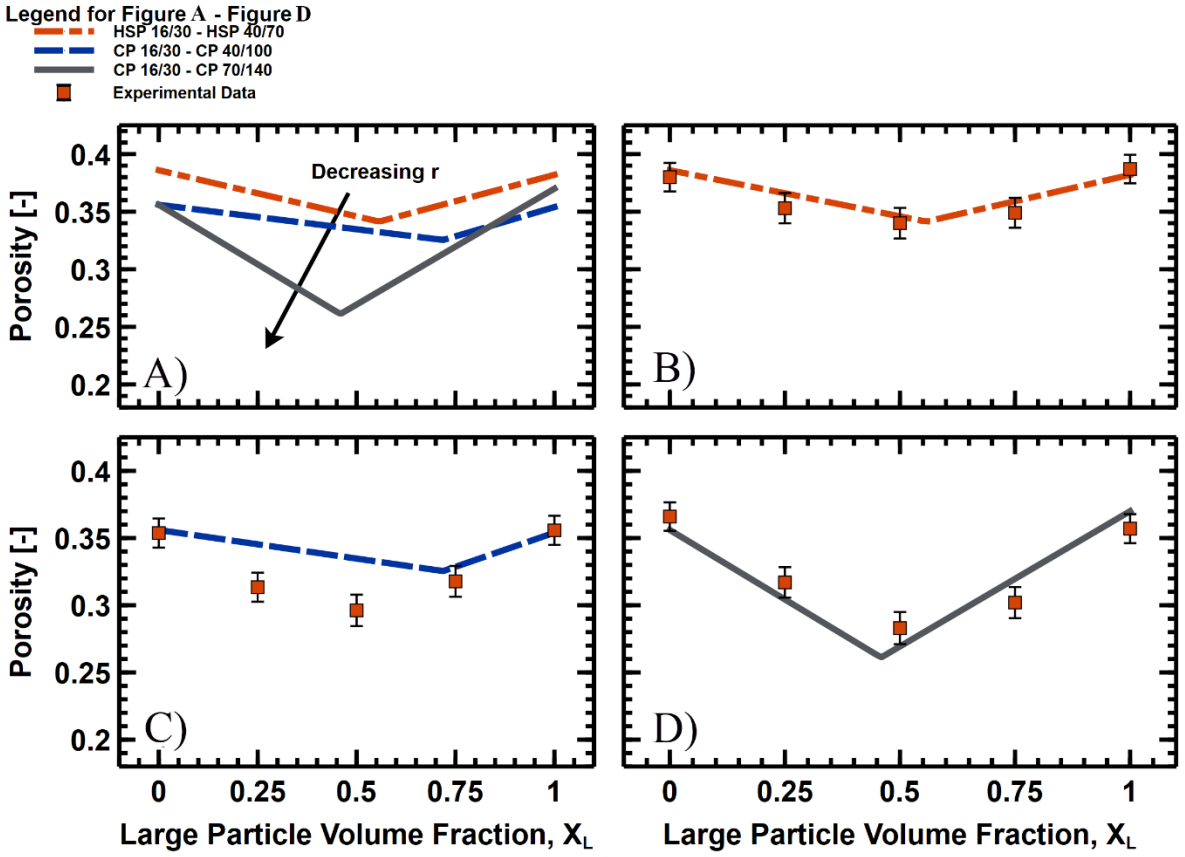

Figure 4. Comparison of theoretical (using the Chang and Deng model) and measured particle porosity: A) Porosity as a function on large particle volume fraction for each of the binary particle systems tested. B-D) Porosity as a function of large particle volume fraction for HSP 16/30 – HSP 40/70, CP 16/30 – CP 40/100, and CP 16/30 – CP 70/140, respectively.

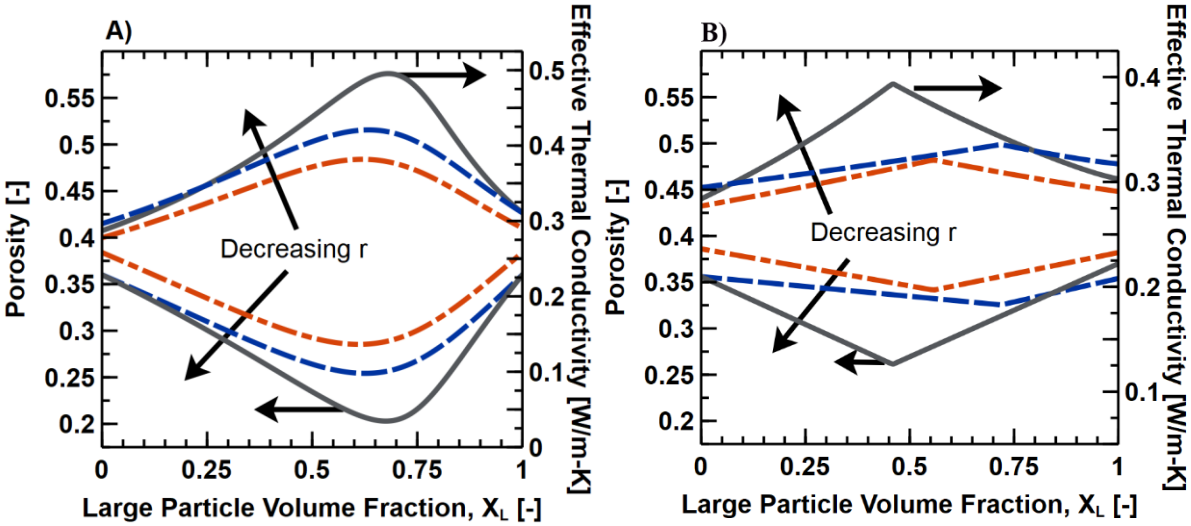

Figure 5. A) Theoretical Yu & Standish porosity (left axis) and ZBS thermal conductivity @ 100 °C (right axis) and B) Change and Deng porosity (left axis) and ZBS thermal conductivity @ 100 °C (right axis) modeled as a function of large particle volume fraction for the bimodal particle mixtures CP 16/30 – CP 70/140 (grey solid line), CP 16/30 – CP 40/100 (blue dashed line), and HSP 16/30 – HSP 40/70 (orange dot-dashed).

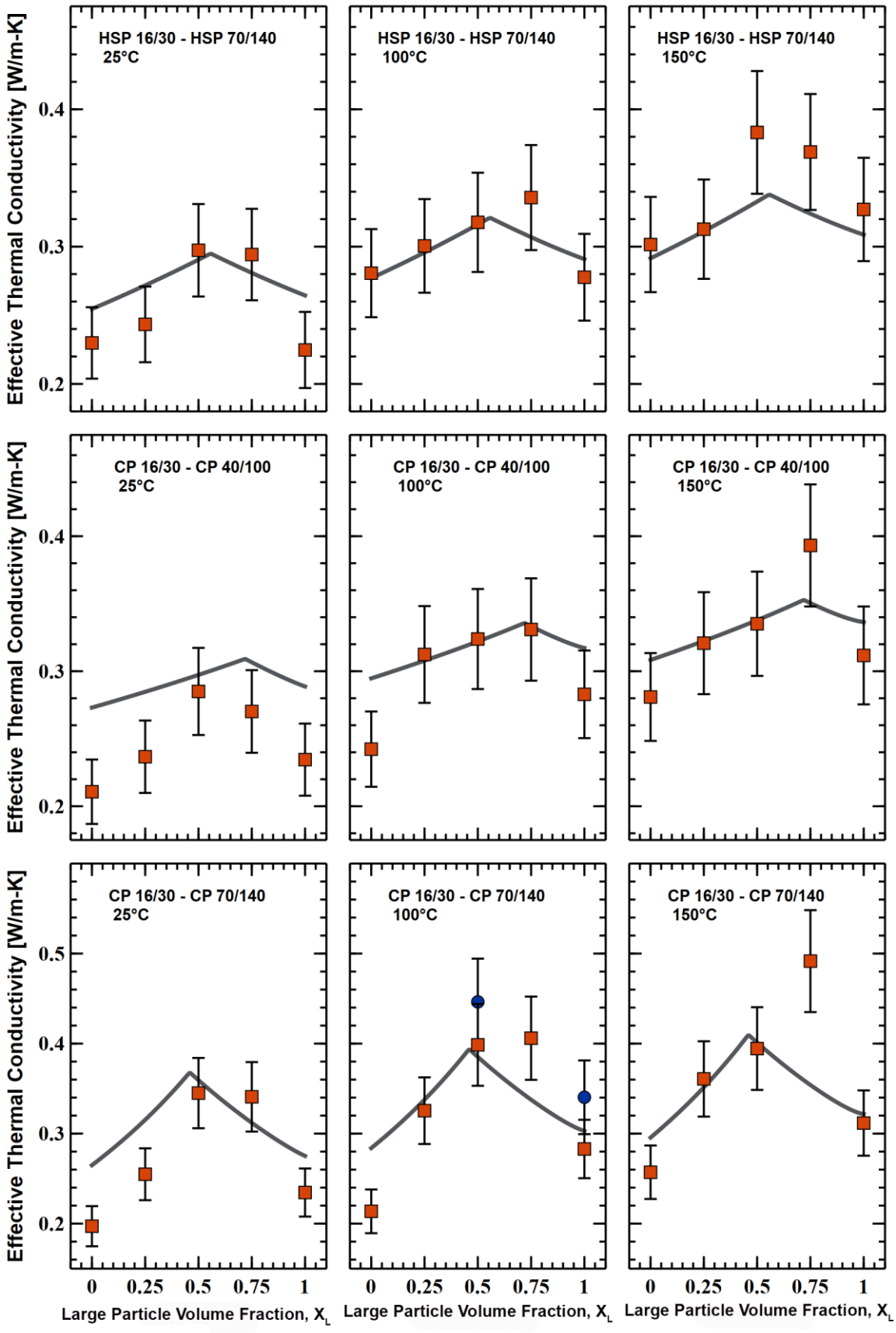

Figure 6. Thermal conductivity results compared to the ZBS model (using the Chang and Deng porosity model) for each particle mixture at temperatures 25, 100, and 150 °C. Orange Squares – TEMPOS; Blue Circles – Thermtest.

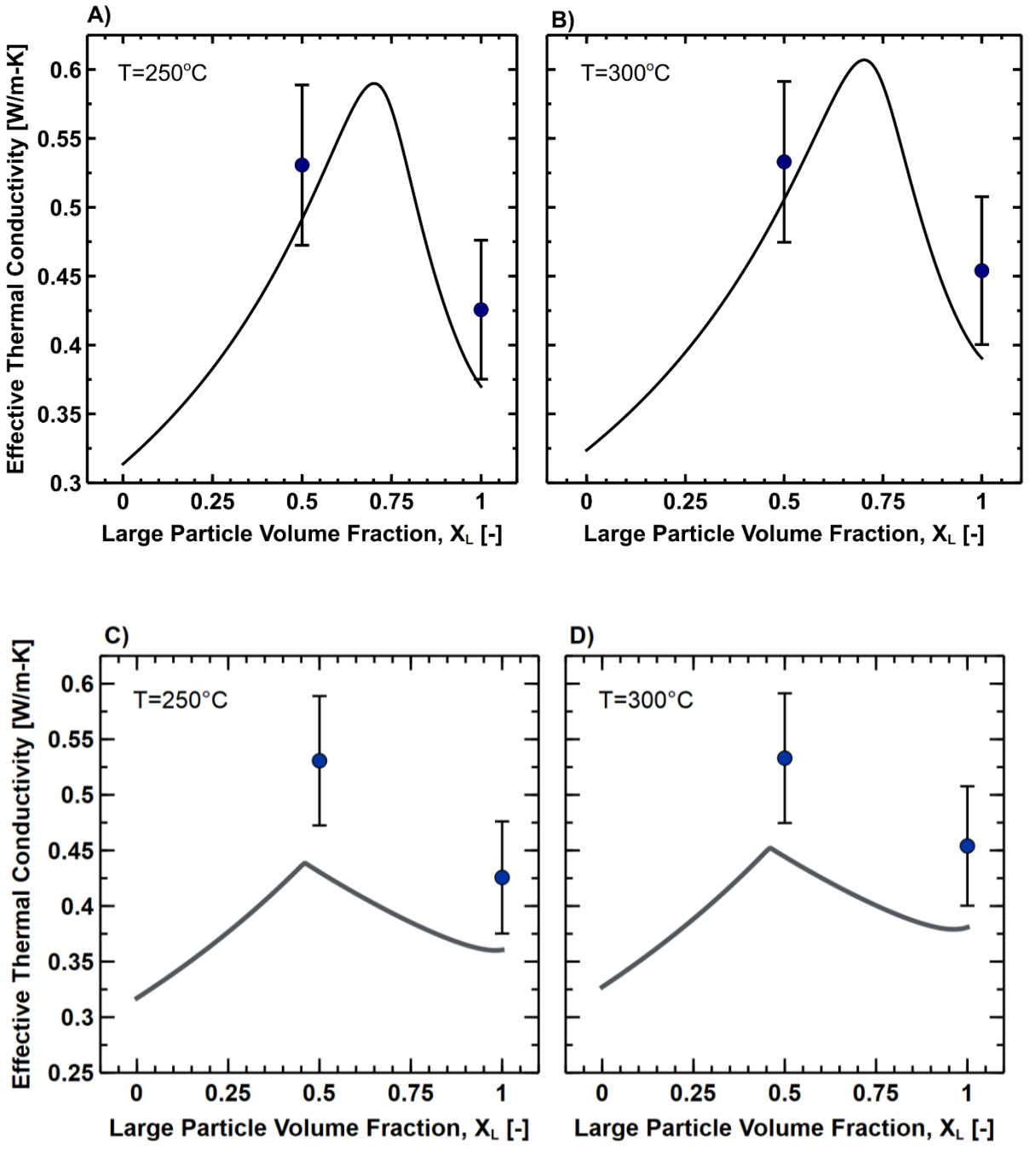

Figure 7. Experimental Packed Bed Effective Thermal Conductivity of CP 16/30 – CP 70/140 Mixtures and Theoretical Model results. A-B) Comparison of experimental results to ZBS model with Standish and Yu porosity model at 250°C and 300°C respectively, C-D) Comparison of experimental results to ZBS model with Chang and Deng porosity model at 250°C and 300°C respectively.

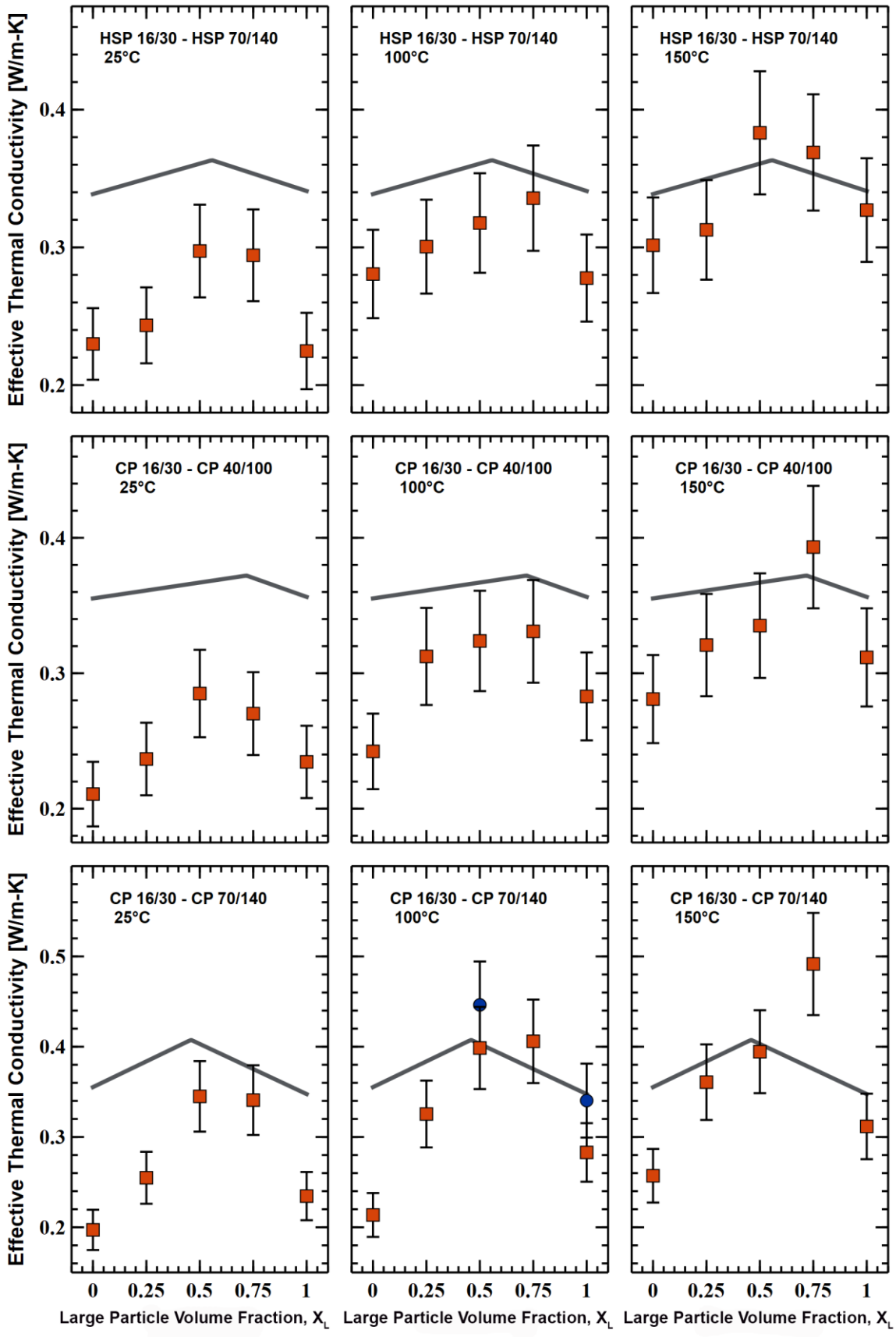

Figure 8. Thermal conductivity results compared to the Yagi and Kunii model (using the Chang and Deng porosity model) for each particle mixture at temperatures 25, 100, and 150 °C. Orange Squares – TEMPOS; Blue Circles – Thermtest.

Appendix A: Particle Size Distributions

The particle distributions for CP 16/30, CP 40/100, CP 70/140, HSP 16/30, and HSP 40/70 were taken from [31] or provided by Carbo during the purchase of the particles. The bimodal particle distributions for all the binary particle systems were calculated as follows:

$$Q_{i,binary} = X_L Q_{i,L} + (1 - X_L) Q_{i,s}$$

where $Q_{i,L}$ is the volume fraction of the coarse component, $Q_{i,s}$ is the volume fraction of the fine component, and X_L is the large particle volume fraction.

Table A.1 Particle size distribution as given by weight percentage retained by each sieve for each of the monodisperse and binary particle systems tested in this study.

Sieve Mesh Size (Microns)	8 - 12 (2360 - 1700)	12 - 16 (1700 - 1180)	16 - 20 (1180 - 850)	20 - 30 (850 - 600)	30 - 40 (600 - 425)	40 - 50 (425 - 300)	50 - 70 (300 - 212)	70 - 100 (212 - 149)	100 - 140 (149 - 105)	140 - 200 (105 - 74)
CP 16/30	0	3	74	23	0	0	0	0	0	0
CP 40/100	0	0	0	0	0	37	45	16	2	0
CP 70/140	0	0	0	0	0	0	1	51	43	5
HSP 16/30	0	3	85	12	0	0	0	0	0	0
HSP 40/70	0	0	0	0	0	48.1	51	0.8	0.1	0
CP 16/30 - CP 40/100 X_L=0.25	0	0.75	18.5	5.75	0	27.75	33.75	12	1.5	0
CP 16/30 - CP 40/100 X_L=0.50	0	1.5	37	11.5	0	18.5	22.5	8	1	0
CP 16/30 - CP 40/100 X_L=0.75	0	2.25	55.5	17.25	0	9.25	11.25	4	0.5	0
CP 16/30 - CP 70/140 X_L=0.25	0	0.75	18.5	5.75	0	0	0.75	38.25	32.25	3.75
CP 16/30 - CP 70/140 X_L=0.50	0	1.5	37	11.5	0	0	0.5	25.5	21.5	2.5
CP 16/30 - CP 70/140 X_L=0.75	0	2.25	55.5	17.25	0	0	0.25	12.75	10.75	1.25
HSP 16/30 - HSP 40/70 X_L=0.25	0	0.75	21.25	3	0	36.075	38.25	0.6	0.075	0
HSP 16/30 - HSP 40/70 X_L=0.50	0	1.5	42.5	6	0	24.05	25.5	0.4	0.05	0
HSP 16/30 - HSP 40/70 X_L=0.75	0	2.25	63.75	9	0	12.025	12.75	0.2	0.025	0

Appendix B: Thermal Conductivity Results

All the monodisperse particles and binary particle systems were tested using the unattended measurement mode on the TEMPOS at temperatures of 25, 100, and 150 ℃ with the following test parameters: Mode: Conductivity/Resistivity, Sensor: TR-3, Power Mode: High (~3.6W), Read Time: One Minute (30 seconds heating and 30 seconds cooling), Interval Time: 15 min.

For both particle samples tested on the Thermtest, the following test parameters were used: Test Power: 0.1W, Test Time: 20 seconds, Calculations Window: 50 to 200 points, Sensor: HTK 5501 F1.

Table B.1 Thermal conductivity results for HSP 16/30 – HSP 40/70 for each temperature and particle system. Modeled results based upon ZBS thermal conductivity model.

Material	Temperature (°C)	$k_{eff,S-Y}$ [W m^{-1}K^{-1}]	$k_{eff,C-D}$ [W m^{-1}K^{-1}]	$k_{eff,experiment}$ [W m^{-1}K^{-1}]	% Difference S-Y	% Difference C-D
HSP 40/70	25	0.256	0.255	0.23	11.30%	10.70%
HSP 16/30 – HSP 40/70, X_L = 0.25		0.292	0.272	0.243	20.16%	11.85%
HSP 16/30 – HSP 40/70, X_L = 0.50		0.323	0.290	0.297	8.75%	2.19%
HSP 16/30 – HSP 40/70, X_L = 0.75		0.315	0.281	0.294	7.14%	4.46%
HSP 16/30		0.263	0.264	0.225	16.89%	17.54%
HSP 40/70	100	0.279	0.277	0.281	0.71%	1.41%
HSP 16/30 – HSP 40/70, X_L = 0.25		0.317	0.296	0.301	5.32%	1.75%
HSP 16/30 – HSP 40/70, X_L = 0.50		0.35	0.316	0.318	10.06%	0.58%
HSP 16/30 – HSP 40/70, X_L = 0.75		0.343	0.307	0.336	2.08%	8.66%
HSP 16/30		0.289	0.291	0.278	3.96%	4.64%
HSP 40/70	150	0.293	0.291	0.302	2.98%	3.48%
HSP 16/30 – HSP 40/70, X_L = 0.25		0.333	0.311	0.313	6.39%	0.57%
HSP 16/30 – HSP 40/70, X_L = 0.50		0.368	0.333	0.383	3.92%	13.11%
HSP 16/30 – HSP 40/70, X_L = 0.75		0.361	0.324	0.369	2.17%	12.20%
HSP 16/30		0.307	0.309	0.327	6.12%	5.60%

Table B.2 Thermal conductivity results for CP 16/30 – CP 40/100 for each temperature and particle system. Modeled results based upon ZBS thermal conductivity model.

Material	Temperature (°C)	$k_{eff,S-Y}$ [W m^{-1}K^{-1}]	$k_{eff,C-D}$ [W m^{-1}K^{-1}]	$k_{eff,experiment}$ [W m^{-1}K^{-1}]	% Difference S-Y	% Difference C-D
CP 40/100	25	0.27	0.273	0.211	27.96%	29.41%
CP 16/30 – CP 40/100, X_L = 0.25		0.326	0.285	0.237	37.55%	20.15%
CP 16/30 – CP 40/100, X_L = 0.50		0.404	0.297	0.285	41.75%	4.32%
CP 16/30 – CP 40/100, X_L = 0.75		0.426	0.307	0.27	57.78%	13.56%
CP 16/30		0.284	0.289	0.235	20.85%	22.85%
CP 40/100	100	0.291	0.295	0.242	20.25%	21.78%
CP 16/30 – CP 40/100, X_L = 0.25		0.351	0.308	0.312	12.50%	1.33%
CP 16/30 – CP 40/100, X_L = 0.50		0.434	0.322	0.324	33.95%	0.60%
CP 16/30 – CP 40/100, X_L = 0.75		0.458	0.333	0.331	38.37%	0.68%
CP 16/30		0.312	0.317	0.283	10.25%	12.08%
CP 40/100	150	0.305	0.308	0.281	8.54%	9.72%
CP 16/30 – CP 40/100, X_L = 0.25		0.366	0.322	0.321	14.02%	0.44%
CP 16/30 – CP 40/100, X_L = 0.50		0.452	0.338	0.335	34.93%	0.84%
CP 16/30 – CP 40/100, X_L = 0.75		0.478	0.350	0.393	21.63%	10.82%
CP 16/30		0.331	0.336	0.312	6.09%	7.81%